Metallogr. Microstruct. Anal. (2013) 2:1–12
DOI 10.1007/s13632-012-0056-2

TECHNICAL ARTICLE

Characterization of Engineered Nickel-Base Alloy Surface Layers Produced by Additive Friction Stir Processing

J. Rodelas · J. Lippold

Received: 20 November 2012 / Revised: 17 December 2012 / Accepted: 17 December 2012 / Published online: 8 January 2013

Abstract Additive friction stir processing (AFSP) was used as a novel method to create consolidated γ'-strengthened superalloy surface layers on non-age-hardenable Ni-alloy substrates. A Ni–Cr–Mo superalloy (Haynes Alloy 282) was deposited onto Ni–Cr–Fe alloy (INCONEL^{TM} Alloy 600) plate using a cold-wire gas tungsten arc process and subsequently friction stir processed. Alloy 282 was incorporated into the surface and led to increases in near-surface hardness to levels over 275 $HV_{0.3}$ as-processed. Heat treatment response and precipitate distribution also improved as a result of AFSP. The application of AFSP led to a 2-fold increase in hardness after a direct age heat treatment relative to the as-deposited GTAW weld overlay without AFSP. Enhancement of precipitate formation kinetics was attributed to stored energy from mechanical stirring of the additive Alloy 282 at high temperature. Electron backscatter diffraction and transmission electron microscopy of AFSP regions showed increased dislocation density for low AFSP heat input processing parameters.

Keywords Friction stir · Additive manufacturing · Superalloy · Misorientation · Nickel alloy

Introduction

The physical properties of a material determine the fitness for a specific purpose or application. In demanding applications, costly high-performance materials are often implemented to satisfy rigorous design requirements. However, the properties of such high-performance materials may only be required in certain locations within a component. The development of site-specific material modification techniques allow for local enhancement of material properties and performance.

Friction stir processing (FSP), a derivative of friction stir welding (FSW), is a solid-state thermomechanical process used for localized, surface microstructural modification. This process has been applied extensively to aluminum alloys to enhance superplastic formability, improve fatigue life, homogenize and refine castings, improve formability, repair cracking and porosity, and fabricate surface composite structures [1, 2]. As with FSW, conventional FSP is generally regarded as an autogenous (i.e., no filler metal) process. However, additive techniques can be applied to FSP to locally change composition and/or constituent phases to ultimately create unique microstructures not otherwise achievable by either FSP or additive techniques alone. The addition of other materials via additive friction stir processing (AFSP) has been explored previously in several studies [3–5]. However, such studies were performed using relatively low-T_m material systems, such as Al-alloys. AFSP in high-T_m systems such as Ni-base alloys has not been studied to any extent despite numerous potential property and performance benefits.

Reported conventional FSP studies of high-T_m alloys, such as Ni-alloys, is extremely limited [6, 7]. Furthermore, AFSP studies pertaining to Ni-base alloys are non-existent and require further study. The solid-state nature of AFSP is expected to result in a superior microstructure compared to existing site-specific fusion-based additive techniques used for Ni-alloys including laser engineered net shaping (LENS), thermal spray, etc. However, even some solid-state processes such as cold spray, selective laser sintering,

J. Rodelas (✉) · J. Lippold
Welding and Joining Metallurgy Group, Welding Engineering Department, The Ohio State University, 1248 Arthur E. Adams Dr., Columbus, OH 43221, USA
e-mail: jmrodel@sandia.gov

laminated object manufacture, etc., cannot obtain fully consolidated final microstructures. As an example of AFSP for Ni-alloys, consider a solid-solution strengthened component used at elevated temperature. Regions of the component subject to high local stresses are susceptible to decreased creep life. Site-specific AFSP can be used to locally modify microstructure and composition. Such regions can be modified in such a way to create local Ni-superalloy regions containing strengthening precipitates that improve room temperature and creep strength. Economic benefit can be gained using AFSP to locally modify the microstructure and properties rather than producing the entire component via special processing or from a costlier alloy.

The objective of this study is to investigate AFSP techniques in Ni-alloy systems to create γ'-strengthened Ni-superalloy surface layers on a non-hardenable Ni alloy substrate. Resulting microstructure, precipitate distribution, and microhardness of AFSP regions are characterized in detail as a function of AFSP parameters.

Experimental

A Ni–Cr–Mo superalloy, Haynes Alloy 282, was deposited onto an INCONEL^{TM} Alloy 600 (IN600) substrate. IN600 is a solid-solution strengthened alloy that cannot be strengthened by heat treatment. Table 1 lists the chemical compositions for the alloys used in this study. Alloy 282 was chosen based on availability as a welding filler metal and its moderately high γ' former content, $\sim$3.4 wt.% Al + Ti. A programmable GTA welding machine was used to deposit Alloy 282. Shallow weld overlays of Alloy 282 were produced atop IN600 using a welding speed, current, voltage, and wire feed speed of 1.27 mm/s, 105 A, 9.8 V, 6.56 mm/s, respectively. A total of four overlapping passes approximately 2 mm thick were placed atop a 75 × 150 mm IN600 plate that was 6.3 mm thick. This arrangement allowed for a relatively flat deposition surface that could be subsequently FSP without requiring post-deposition machining.

FSP of the Alloy 282 deposition layer to create AFSP regions was performed on a gantry-style FSW machine using a water-cooled 19 mm shoulder diameter W-25Re tool. The tool pin was a featureless truncated conical pin 3.2 mm in length, which was sufficient to process the approximately 2 mm thick Alloy 282 weld overlay. Argon shielding was used to minimize oxidation of the workpiece during AFSP. Physical simulation of the AFSP thermal cycle was performed on as-deposited Alloy 282 weld overlay using a Gleeble® 3800 (Dynamic Systems Inc., Poestenkill, NY) thermomechanical simulator.

Additive FSP samples with and without post-AFSP aging heat treatments were examined using several techniques. The presence of constituent phases within sectioned and polished specimens selectively etched to reveal precipitates[1] was observed using a high-resolution scanning electron microscopy (HRSEM) equipped with a semi-immersion through lens detector. Additionally, misorientation analyses of AFSP stir zone microstructures were performed using electron backscatter diffraction (EBSD) utilizing an SEM equipped with an EBSD system. Quantitative analysis of local chemical composition was also performed using energy dispersive spectroscopy (EDS) in the SEM. Samples for transmission electron microscopy (TEM) examination were prepared and extracted using focused ion beam milling and in situ extraction. A scanning transmission electron microscope (STEM) was used for examination of FIB prepared specimens.

Microhardness mapping of AFSP regions was performed using an automated hardness tester. A Vickers diamond indenter was used to create arrays of indents using a 300 g applied load. An indent spacing of approximately 250 μm was utilized.

Table 1 Alloy compositions

Element (wt.%)	Alloy 600	Alloy 282
Cr	16.69	19.45
Fe	9.36	1.05
Mn	0.21	0.05
Al	0.188	1.43
Ti	0.22	2.00
Si	0.12	0.10
C	0.08	0.053
B	…	0.004
P	0.005	0.003
S	<0.001	<0.002
Cu	…	<0.01
Mo	…	8.55
Co	…	10.28
Ni	Balance	

Results and Discussion

Additive Friction Stir Processing

A process window was determined for the materials, tool geometry, and workpiece dimensions used in this study.

[1] Chromium(VI) trioxide was added to a mixture of sulfuric and phosphoric acid (2:15 by volume) until saturated. Samples were then etched electrolytically at $\sim$0.5 A/cm^2. Etching time was approximately 30 s. Three-dimensional morphologies of the remaining precipitate phases were observed using a field emission SEM equipped with an asymmetric semi-immersion lens. A scintillation-type through-lens detector (TLD) was used for high-resolution imaging.

Process parameter combinations (i.e., spindle speed and tool traverse speed) selected for further study represent conditions at the extremes of the process window. This resulted in creating AFSP material using a low (100 RPM; 114 mm/min) and a high-heat input parameter combination (150 RPM; 51 mm/min). Selection of the processing window extremes allows observation of all possible microstructures formed for the parameter set previously developed. It can be assumed that microstructural development for intermediate parameter combinations that fall within the processing window will exhibit characteristics between these extremes. Figure 1 shows photographs of AFSP of Alloy 282 on IN600 for both heat input parameter combinations.

Transverse cross sections of AFSP regions reveal the distribution of the additive Alloy 282 within the stir zone (SZ). Light optical micrographs of AFSP cross sections electrolytically etched with 10% oxalic acid to stain Alloy 282-containing regions dark are shown in Fig. 2. Digital image analysis of light optical micrographs reveals 63 and 72% of the added Alloy 282 was incorporated into the SZ for the high- and low-heat input FSP runs, respectively. Alloy 282 not incorporated in the SZ was extruded as flash during AFSP. Although the amount of Alloy 282 incorporated in the SZ for both heat input conditions is similar, the distribution within the stir zone is markedly different due to the difference in material flow characteristics that results from different parameter combinations. The high-heat input parameter combination (Fig. 2a) resulted in a higher degree of intercalation (mixing) and dispersion of additive material within the SZ advancing side (AS). Higher strain rates combined with locally higher temperatures expected on the AS of the tool [2, 8] likely accounts for such behavior. However, less intermixing was observed on the retreating side (RS) of the SZ. Within the RS, the additive material appears to exist in a large contiguous region. The rather linear boundary between Alloy 282/IN600 on the RS compared to the tortuous boundary that exists on the AS suggests the degree of turbulence and material flow is lower on the RS. Additionally, accumulation of Alloy 282 on the RS is considerably more pronounced, especially for the high-heat input condition (Fig. 2a). Moreover, the fraction of additive material on the AS is considerably lower compared to the RS which suggests that additive material picked up by the front of the tool on the AS is transported and deposited behind the tool on the RS.

Overall, the distribution of additive material for the low-heat input parameter combination (Fig. 2b) suggests more turbulent material flow compared to AFSP with high-heat input parameters. While both parameter combinations do not exhibit a large degree of flow parallel to the plate thickness direction, evidence of some downward flow of Alloy 282 was observed in etched cross sections. Macrographs of the AFSP SZ regions (Fig. 2) that show the upper layer in the SZ, approximately 200–250 μm thick, is composed of light-etching IN600 rather than the additive Alloy 282, despite the addition of Alloy 282 to the topmost surface in the initial condition before FSP. Likely, the formation of a layer of substrate material on the top surface is an artifact of the particular tool geometry used.

Dilution of the additive material by the substrate was not observed. A quantitative EDS line scan of the turbulent

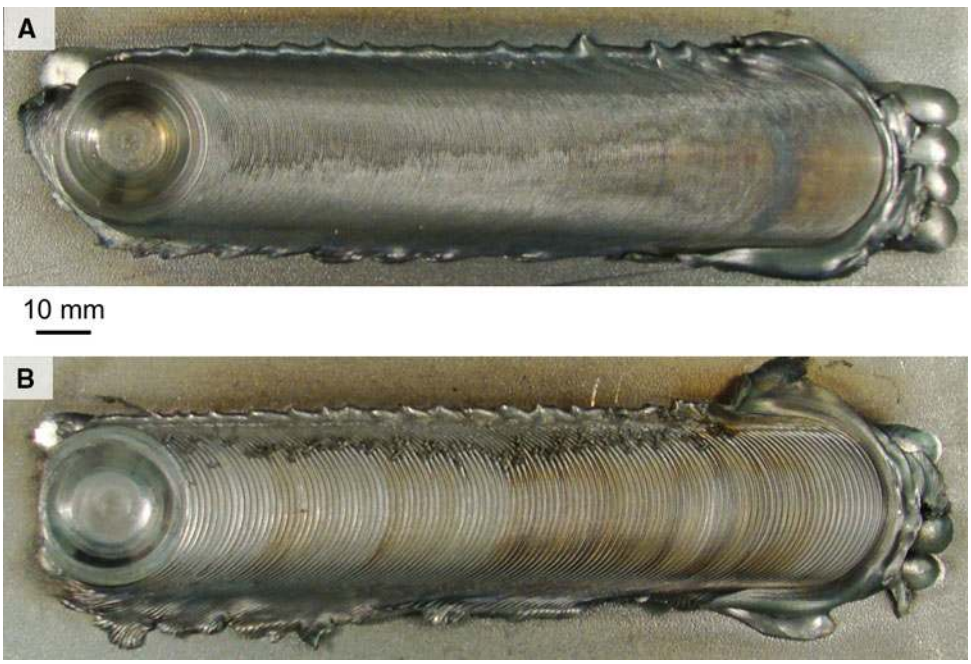

Fig. 1 Photographs of AFSP Alloy 282 on Alloy 600 processed using **a** high-heat input parameter combination (150 RPM/51 mm/min) and **b** low-heat input (100 RPM/114 mm/min)

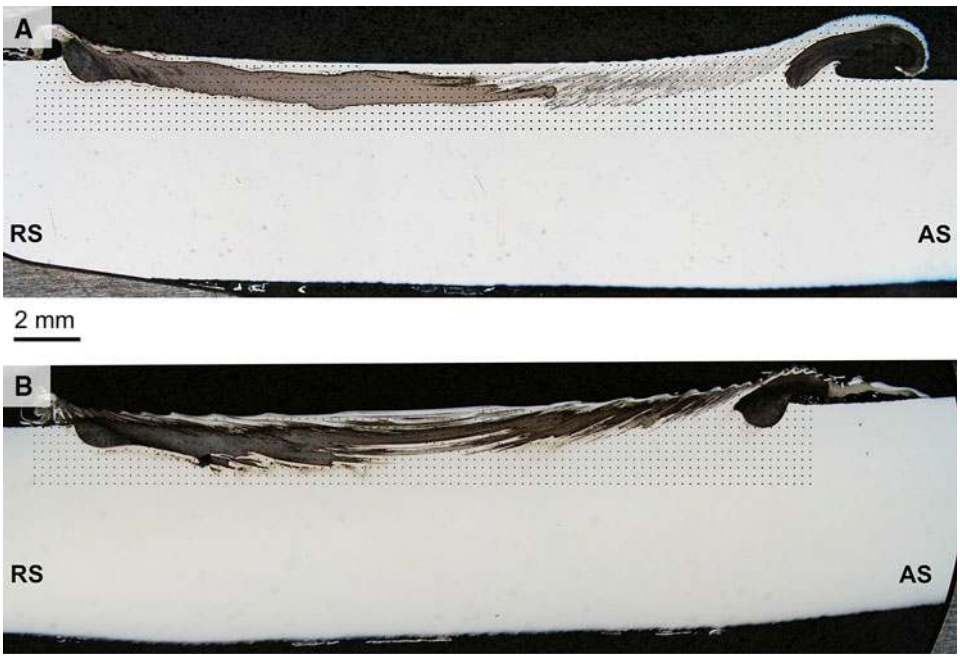

Fig. 2 Light optical micrographs of transverse cross section of AFSP regions for **a** high-heat input and **b** low-heat input parameter combinations. Samples electrolytically etched with 10% oxalic acid. Alloy 282 appears as dark-etching regions

Alloy 282-containing SZ AS processed using low-heat input parameters shows little dilution of Alloy 282 despite intermixing of materials (Fig. 3a). Transitions from IN600 to Alloy 282 along the trace result in very abrupt changes in the quantified concentrations of Co and Mo, which are not present in IN600 (Fig. 3b). This result suggests that dissimilar surface layers can be produced via AFSP with minimal dilution by the substrate.

Microstructure and Hardness of AFSP Regions

Microhardness maps of the AFSP SZ indicate increased hardness within the SZ for regions that are predominantly Alloy 282-containing. Figure 4 shows the hardness distribution in the AFSP SZ regions for both parameter combinations. AFSP Alloy 282-containing regions of the microstructure exhibit hardness values of 275 $HV_{0.3}$ or greater depending on location and process parameters. The as-deposited hardness of the original Alloy 282 deposit layer is 205 ± 13 $HV_{0.3}$, comparable to the hardness of FSP IN600 (180–200 $HV_{0.3}$) and IN600 base material (186 ± 6 $HV_{0.3}$).

For both parameter combinations, the more turbulent AS exhibits slightly higher hardness compared to the RS. Interestingly, the sample processed using low-heat input parameters (Fig. 4b), contains the highest hardness regions despite lower peak process temperatures and higher cooling rates. Some regions within the SZ exceed 300 $HV_{0.3}$. Measurements from ANSI Type-K thermocouples embedded adjacent to the SZ indicate temperature for material processed using the low-heat input parameters reached a

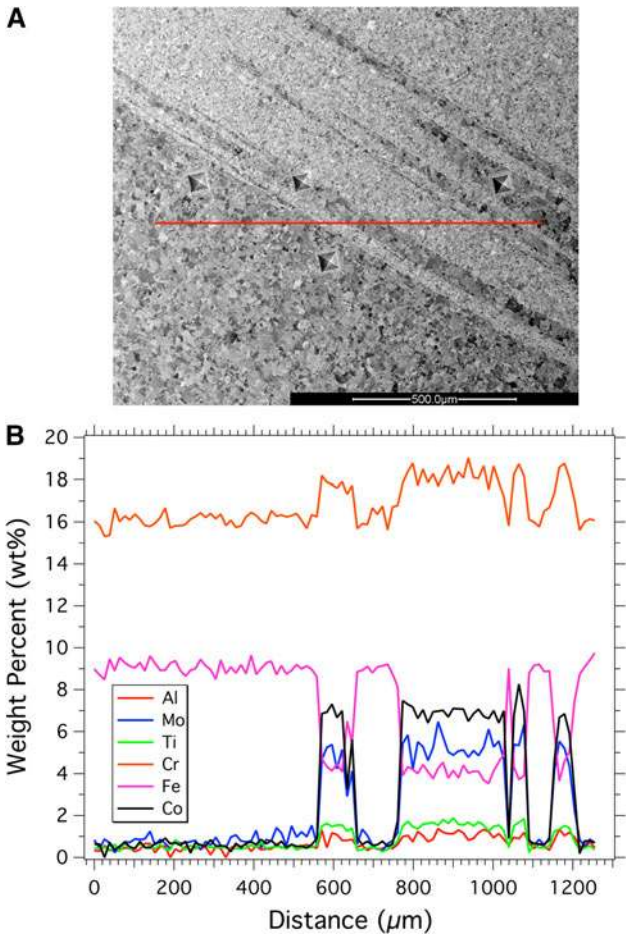

Fig. 3 **a** EDS line scan trace performed in the SZ region. **b** Corresponding composition profile for trace shown in (**a**)

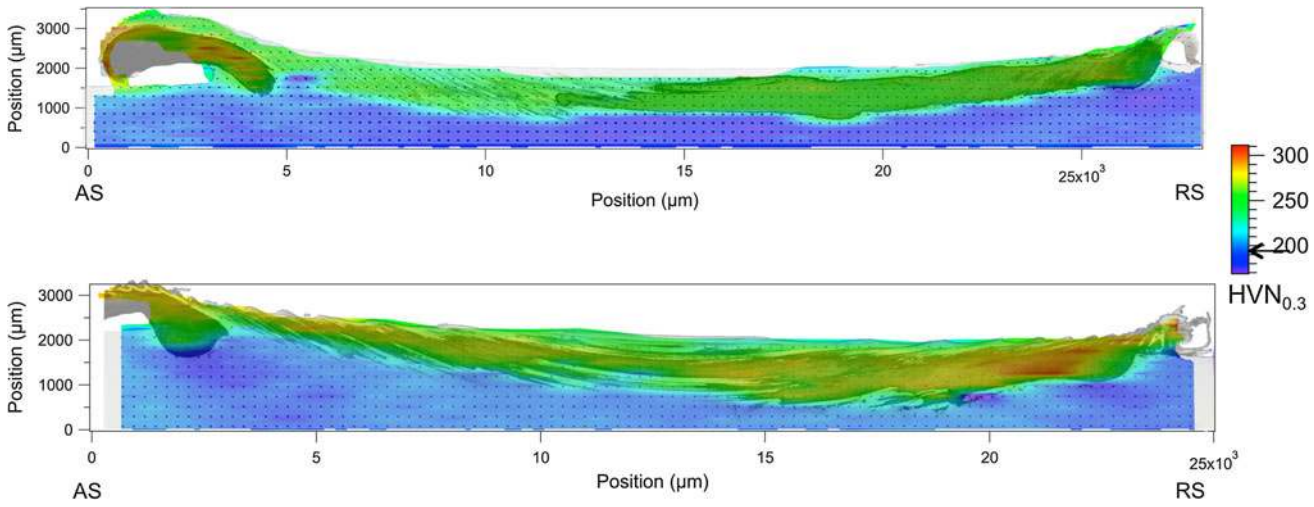

Fig. 4 Microhardness maps of AFSP regions for **a** high-heat input and **b** low-heat input parameter combinations

peak of 895 °C; approximately 200 °C lower than the high-heat input condition. Additionally measured cooling rates of the low-heat input sample were nearly double (36 °C/s) compared to the high-heat input sample (19 °C/s).

High-resolution SEM of selectively etched AFSP samples reveals a refined recrystallized microstructure with no evidence of the solidification structure remaining from the original weld overlay (Fig. 5). Also present in some regions near the edge of the Alloy 282-containing SZ is a lamellar distribution of fine precipitates that correspond to high hardness regions (Fig. 4). Additive FSP material processed using the low-heat input process parameters contained a larger fraction of fine SZ precipitates compared to the high-heat input condition. Upon closer examination (Fig. 5d), these lamellar regions contain clusters of fine precipitates ranging in size from 15 to 125 nm. The majority of the particles have rounded or slightly cuboidal morphology typical of γ' formed during relatively fast cooling [9]. Precipitate-containing regions also have submicron grains (Fig. 5d). The formation of sub-micron grains within these regions is likely due to a modification of the grain coarsening processes via Zener pinning by precipitates or solute drag from alloying additions in Alloy 282 [10]. A similar refining phenomenon has been observed during FSW of Al–Mg–Sc alloys [11]. The combination of a fine precipitate distribution combined with Hall–Petch strengthening from grain refinement likely contributes to the high hardness in some regions of the AFSP SZ.

Samples of as-deposited material were thermally cycled using simulated thermal histories that mimic measured AFSP thermal cycles to determine the evolution of the as-deposited microstructure in the absence of deformation. A Gleeble® thermomechanical simulator was used for physical simulation of both heat input conditions. The resulting microstructure of the thermally simulated as-deposited weld overlay is shown in Fig. 6. Because no deformation occurred during Gleeble thermal simulation, the solidification microstructure characteristic of the as-deposited weld overlay persists. Large (>100 μm) solidification grains are observed for both conditions. However, unlike the as-deposited, non-cycled Alloy 282, both simulation conditions exhibit the presence of bright clusters of particles present within interdendritic regions when selectively etched.

Closer inspection of the interdendritic particle clusters for the low-heat input cycle sample (Fig. 6b) indicates regions containing fine (approximately 10–20 nm) spherical particles. These fine particles are morphologically similar to secondary γ' which forms during a rapid thermal excursion. The formation of pockets of fine γ' is the result of enrichment of γ'-promoting elements (e.g., Al + Ti) at the interdendritic regions during solidification of the weld overlay. The same phenomenon, described in the following sections of this article, is also responsible for the locally heterogeneous age hardening response of the as-deposited Alloy 282.

Low-magnification micrographs for the high-heat input thermal cycle sample also show clusters of particles within along the dendrite boundaries (Fig. 6c). However, closer examination of particles within these clusters (Fig. 6d) reveals a morphology that is unlike the secondary γ' found in the low-heat input condition. The particles present are a mixture of irregularly shaped, globular particles 100–500 nm in size along with some blocky submicron particles. Such a morphology is not characteristic of secondary γ' formed upon cooling.

The measured FSP thermal profiles used to create the thermal simulation samples differ in cooling rate as

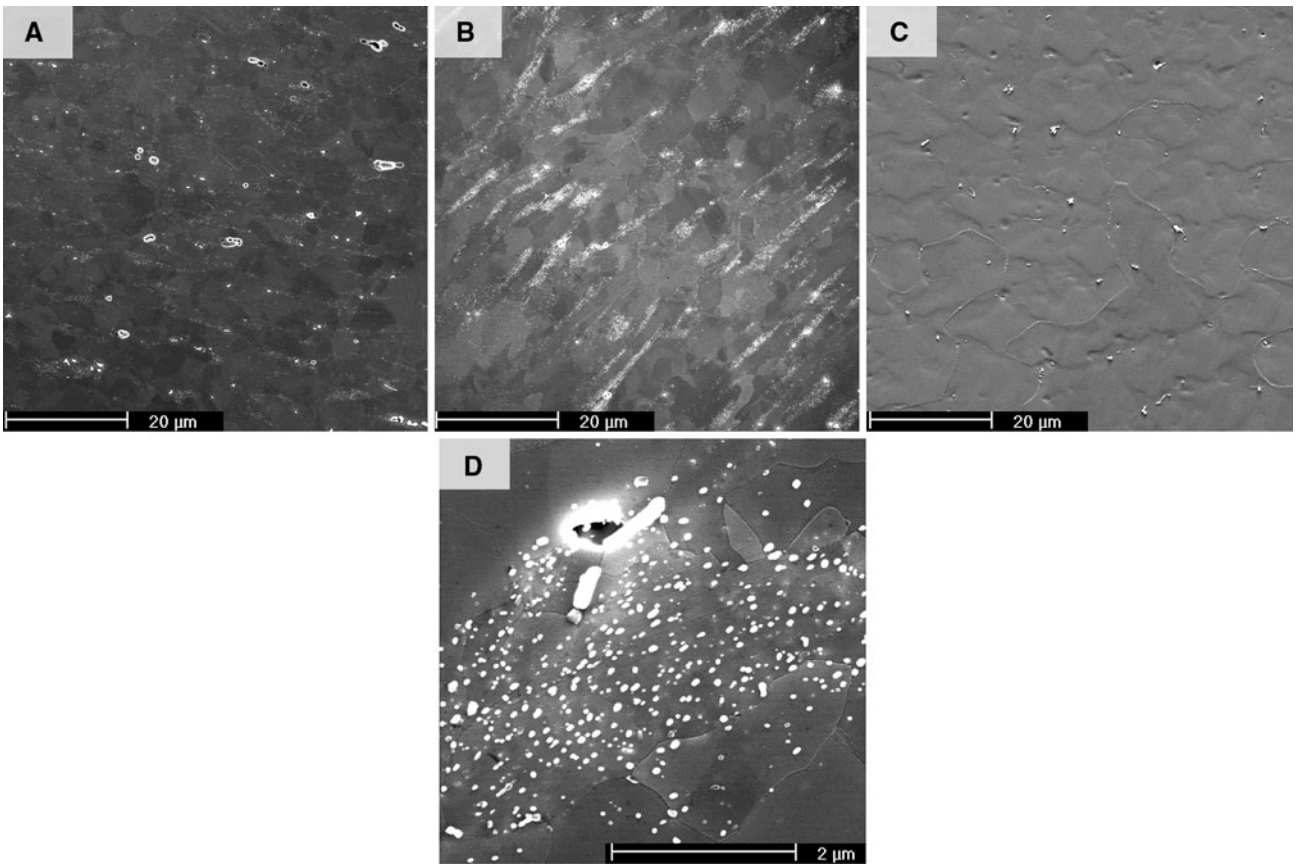

Fig. 5 Electron micrographs of selectively etched AFSP SZ regions processed using **a** high-heat input and **b** low-heat input, **c** as-deposited Alloy 282, **d** higher magnification of a precipitate-containing region in AFSP sample using low-heat input parameters

described previously. In addition, thermal cycles differ in peak temperature relative to the γ' solvus temperature of 1006 °C as predicted using JMatPro,[2] which is in good agreement with an experimentally derived solvus temperature of 997 °C [12]. As a result, the peak process temperatures for the high (1093 °C)- and low (895 °C)-heat input AFSP cycles represent cycles that are super- and subsolvus, respectively, for γ'.

In the as-deposited condition titanium partitions strongly to the liquid during solidification of Alloy 282 [13]. Despite the resulting local interdendritic enrichment of titanium, the rapid cooling associated with the GTAW weld overlay process suppresses the formation of γ', thereby retaining the titanium in solution. During the low-heat input FSP thermal cycle, the peak temperature remains below the γ' solvus and cools through the γ' precipitation temperature range. Although the simulated cooling rate is rapid ($\sim$40 °C/s from 800 to 600 °C), fine, secondary γ' still forms within the Ti-rich regions.

The high-heat input sample, however, differs from the low-heat input cycle in that the slower traversing tool results in a thermal cycle that remains supersolvus with respect to γ' for approximately 12 s. Upon exposure to temperatures above the γ' solvus temperature for even brief durations, Ti-enriched regions in the weld metal microstructure preferentially form Ti-rich carbides and carbonitrides [14]. The formation of these Ti-rich compounds consumes solute from the surrounding region. When the material is then cooled through the γ' precipitation temperature range, the interdendritic regions are now considerably leaner in Ti due to carbide and carbonitride formation. Despite slower cooling rates associated with the high-heat input condition, γ' formation is suppressed due to the lower Ti content of the matrix.

The results of thermal simulations suggest that the formation of fine clusters of spheroidal precipitates observed within some regions of the as-AFSP SZ result from regions of the original weld overlay that are deformed such that mechanical mixing is not sufficient to completely homogenize solute segregated regions thus leading to the distribution of lamellar precipitate-containing areas for some regions of the SZ.

[2] JMatPro (Sente Software Ltd., Guildford, UK) version 5.1.1, Ni-superalloy database.

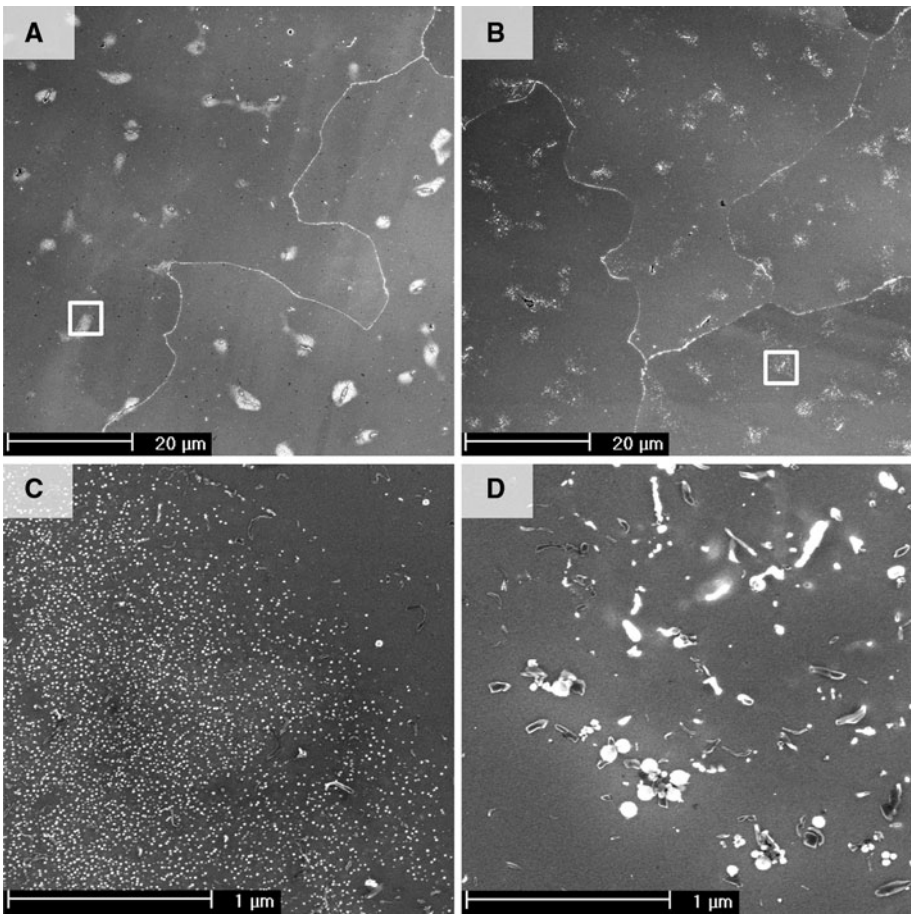

Fig. 6 HRSEM micrographs of selectively etched thermally simulated Haynes Alloy 282. **a** and **b** Regions of low-heat FSP input simulated weld overlay microstructure; **c** and **d** weld overlay of simulated high-heat FSP input

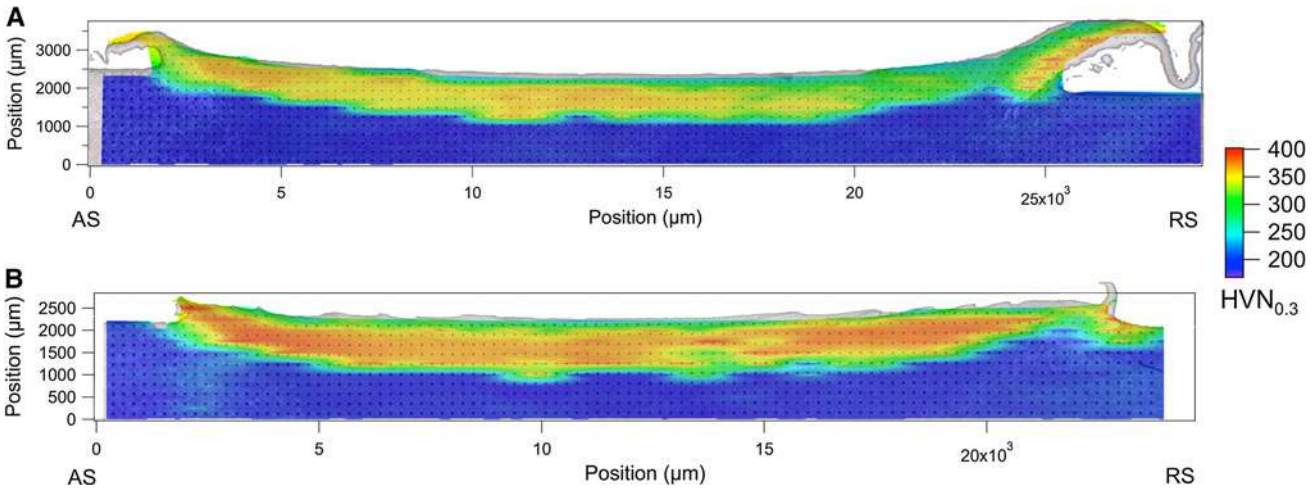

Fig. 7 Microhardness maps of AFSP regions after 2 h heat treatment at 750 °C for **a** high-heat input and **b** low-heat input parameter combinations

Heat-Treatment Response of AFSP Material

The addition of Alloy 282 using AFSP creates an age-hardenable superalloy surface layer. The heat treatment response of this layer was explored. Additive FSP samples were subjected to an abbreviated post-AFSP direct age heat treatment of 750 °C for 2 h. Typically a two-step aging heat treatment is used for Alloy 282 which is composed of 1010 °C/2 h/air cool (AC) + 788 °C/8 h/AC [12]. Following heat treatment, both the AFSP conditions exhibited an

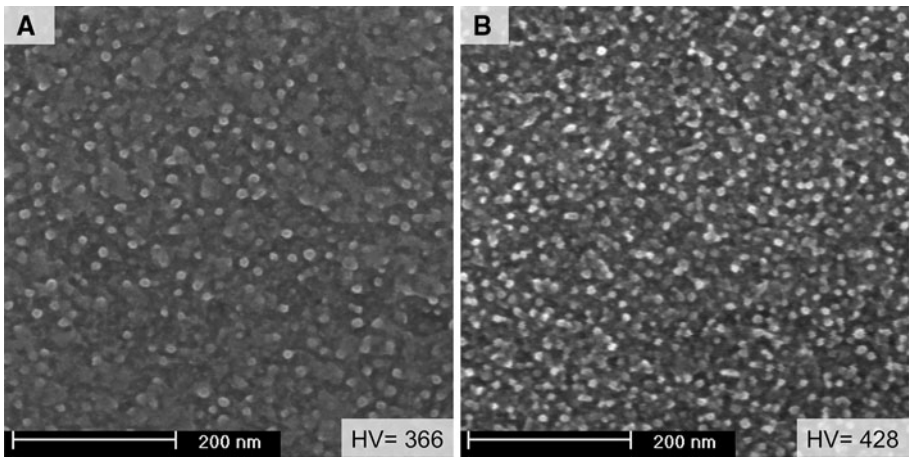

Fig. 8 Distribution of γ' after heat treatment for **a** high-heat input and **b** low-heat input parameter combination

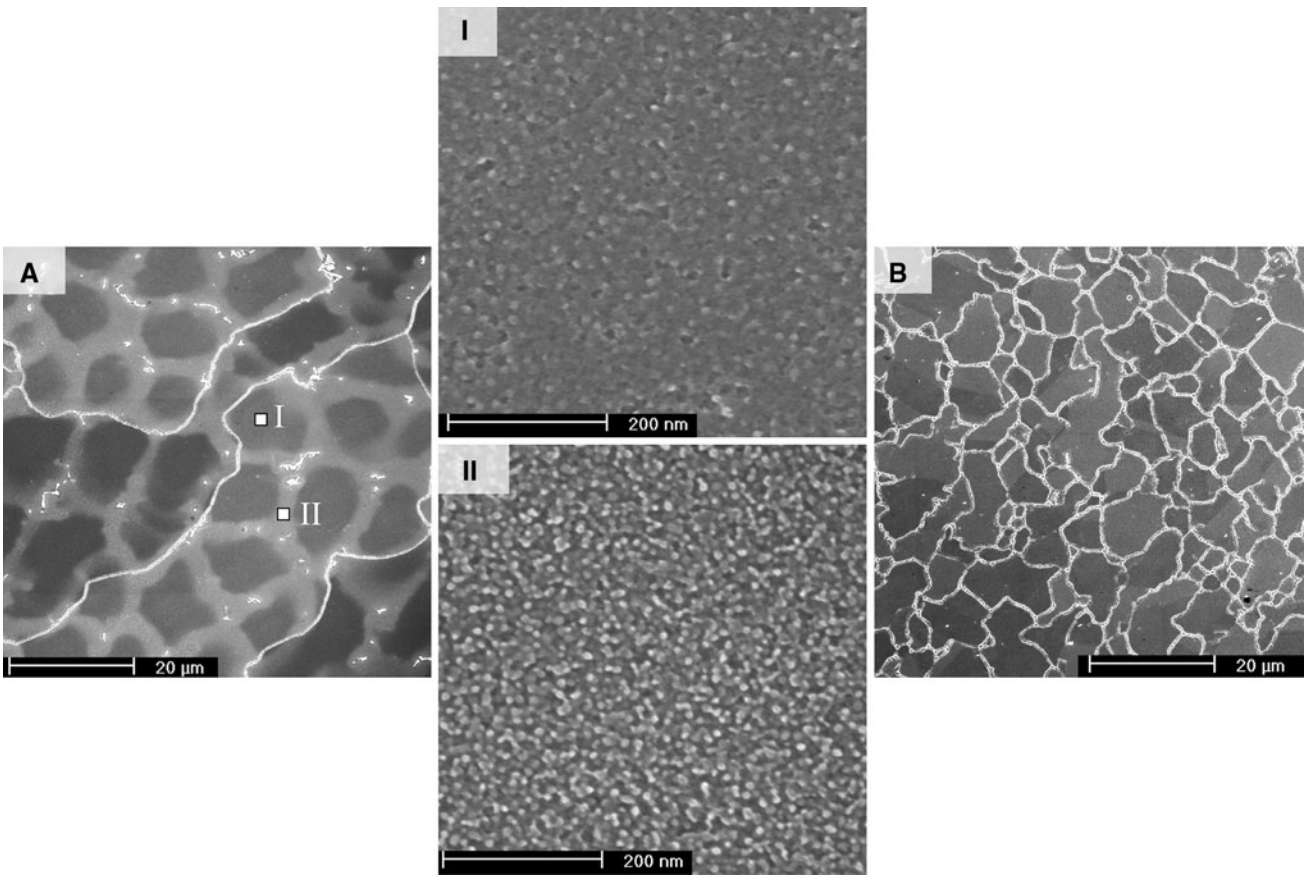

Fig. 9 **a** Locally heterogeneous heat treatment response from microsegregation in as-deposited Alloy 282 demonstrating decreased fraction γ' in (*I*) dendrite core relative to (*II*) interdendritic region. **b** Heat-treated Alloy 282-containing SZ exhibiting no microsegregation

increase in hardness due to the formation of a fine distribution of γ'. The microhardness distribution within the AFSP SZ after heat treatment is shown in Fig. 7. The average hardness of the Alloy 282 within the AFSP SZ increases to 360 ± 28 and 410 ± 31 $HV_{0.3}$ for high- and low-heat input parameters, respectively. For comparison, the weld overlay of Alloy 282 after heat treatment exhibited a measured average microhardness of 305 ± 13 $HV_{0.3}$, 15–26% lower than AFSP average hardness.

As with the non-heat treated AFSP samples, the AS of the SZ contains the highest proportion of Alloy 282 with high hardness (>400 $HV_{0.3}$). Additive FSP samples processed using low-heat input parameters exhibited the more enhanced heat treatment response despite experiencing

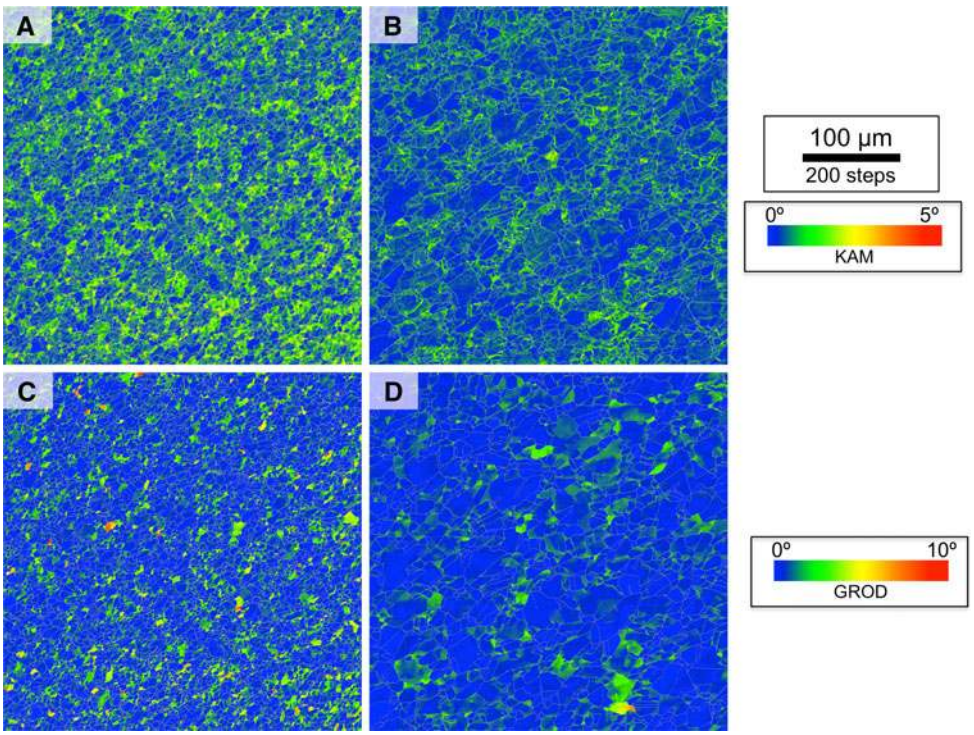

Fig. 10 KAM maps of AFSP SZ for **a** high-heat input and **b** low-heat input parameters. Maps generated using third-order nearest neighbor perimeter kernels. Grain reference orientation deviation maps of AFSP SZ for **c** high-heat input and **d** low-heat input parameters. Intragranular orientation deviation-based relative to the minimum KAM point within the grain

lower peak temperatures during processing and faster cooling rates relative to the high-heat input conditions. The microstructure after heat treatment reveals the formation of fine, spherical γ' within SZ regions with hardness values exceeding $\sim$375 $HV_{0.3}$. Figure 8 shows representative micrographs of the distribution of γ' for the two FSP heat input conditions. The low-heat input sample demonstrated enhanced heat treatment response relative to the high-heat input condition. Volume fraction estimates of γ' using digital image analysis reveal the low-heat input condition contains an average 14.2 vol.% γ' prime compared to the high-heat input conditions which contains on average 8.1 vol.% γ'.

The kinetics of γ' formation in Ni-base superalloys depend on not only time and temperature but also the degree of stored energy in a material in the form of dislocations [15, 16]. An increase in stored energy in the form of dislocations can function to increase the number of heterogeneous nucleation sites for precipitates as well as locally enhance diffusion. The microhardness results of heat-treated AFSP samples suggest process parameter changes, which affect the extent of recovery and recrystallization, influence the amount of stored energy in a material after AFSP.

Without AFSP, the GTAW weld overlay forms microstructures that exhibit locally heterogeneous heat treatment response due to microsegregation of γ' promoters during solidification. Solute partition coefficients less than unity combined with low Al + Ti diffusivity in the γ matrix [17] lead to the formation of interdendritic regions with enhanced heat treatment response relative to the solute lean dendrite core region. Figure 9 demonstrates the heterogeneous distribution of γ' in the Alloy 282 weld overlay after age heat treatment. Regions in the microstructure containing higher γ' fractions appear lighter in the micrographs not due to atomic number contrast, but due to increased electron detector signal from submicron precipitates exposed on the sample surface after selective etching.

Unlike the original weld overlay, the AFSP SZ does not exhibit locally heterogeneous distributions of γ' after aging heat treatment. Mechanical mixing of the additive material at elevated temperature eliminates the original microsegregation of γ' formers thus circumventing homogenization heat treatments typically used to eliminate weld metal compositional heterogeneity. Figure 9(b) demonstrates the typical homogenous distribution of γ' within the SZ of a heat-treated AFSP sample.

Misorientation Analysis of AFSP Regions

Local variations in crystallographic misorientation can serve as indicators of the accumulation of stored dislocations within a material. The presence of dislocation arrays within a material leads to the formation of low angle (<10°) misorientations, which can be characterized via EBSD [18–20]. Point-to-point misorientation can be

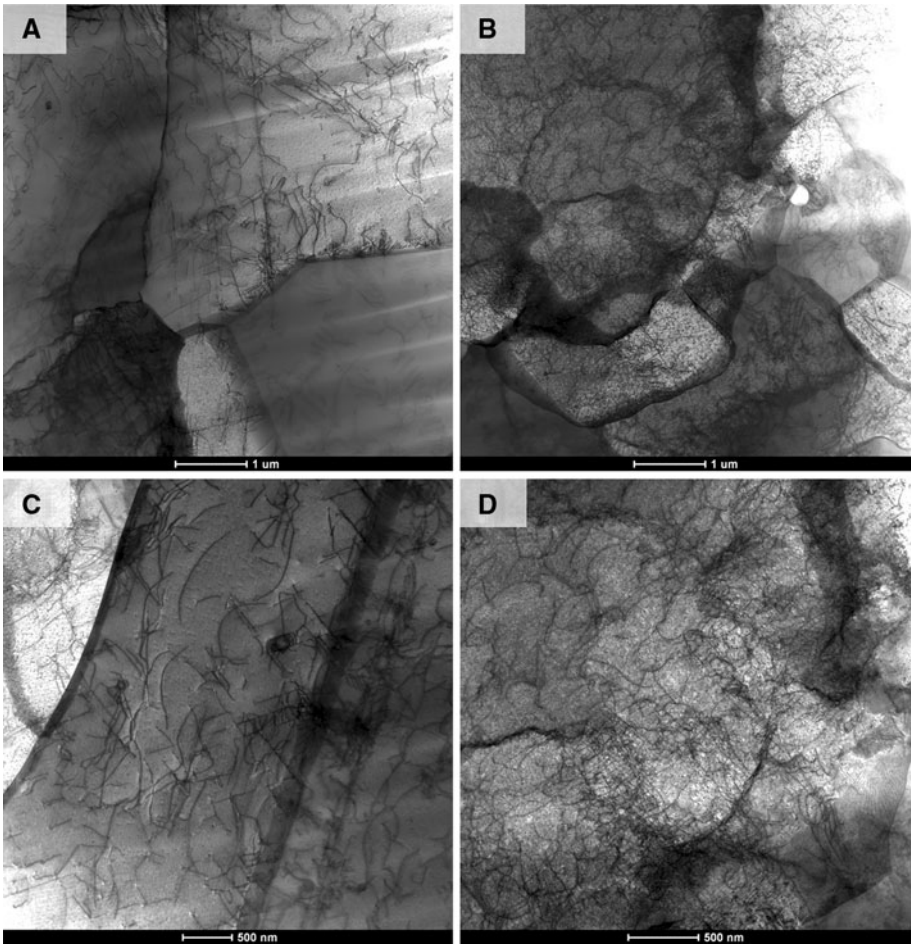

Fig. 11 Low-magnification STEM BF micrographs of **a** high-heat input and **b** low-heat input AFSP Alloy 282. High-magnification STEM BF micrographs showing defect structure in AFSP Alloy 282 processed with **c** high-heat input and **d** low-heat input processing conditions

determined using the kernel average misorientation (KAM) method which determines the average misorientation of a point within an EBSD scan relative to neighboring points. Figure 10 shows KAM maps for Alloy 282-containing regions of the AFSP SZ for both parameter conditions. Regions within the microstructure with very low KAM (blue regions) represent regions of the SZ where recovery and recrystallization processes are complete resulting in very low point-to-point misorientation and therefore low dislocation density. Other regions in the KAM map (shaded green and yellow) correspond to regions of the microstructure with a high density of low-angle misorientation, i.e., stored dislocations. The frequency of such regions is higher overall for the sample processed using low-heat input parameters which suggests that stored energy within the AFSP SZ is higher compared to material processed with high-heat input parameters. Likely, the lower peak temperature during stirring and faster cooling rates behind the tool reduced the extent of recovery/recrystallization compared to material processed at higher peak temperatures with lower cooling rates (high-heat input parameters).

Figure 10(c) and (d) shows grain reference orientation deviation (GROD) maps for both heat input conditions. Grain reference orientation deviation is a measure of intragranular misorientation and is especially useful for visualizing the distribution of misorientation (i.e., stored energy) within the grain [19]. Generated GROD maps indicate a higher fraction of AFSP SZ grains containing higher intragranular misorientations, suggesting such grains contain locally higher stored energy. Grain reference orientation deviation results are in good agreement with the previously discussed point-to-point KAM analyses. While misorientation analyses are not a direct measure of dislocation density, or a quantitative measure of strain within a microstructure, such analyses clearly show the relative difference in stored energy present in AFSP with varied processing parameters. Such differences in stored energy likely account for the observed microhardness trends and aging responses.

Additive FSP Alloy 282 TEM specimens were also extracted from central SZ regions—the same region examined using EBSD. Samples were examined using STEM to directly observe dislocation arrays that led to the misorientation distribution characterized by EBSD. Figure 11 shows low-magnification brightfield STEM micrographs of Alloy 282-containing SZ processed with low- and high-heat input

parameters. Equiaxed grains are clearly observable with the same morphology and range of sizes as measured by EBSD. The intragranular contrast formation observed within some grains is due to local lattice bending and distortion attributed to the presence of dislocations. Such distortion locally changes the diffraction condition and therefore affects the resulting image contrast formation. Larger grains visible in the TEM sample exhibit relatively uniform intragranular contrast which is indicative of low dislocation density. No evidence of fine secondary precipitation was observed in regions contained within TEM specimen, which is consistent with the majority of AFSP SZ material in the as-processed condition when examined using HRSEM. Additional extracted samples in some regions of the SZ may be successful in capturing fine secondary γ', as shown in Fig. 5(d).

Closer examination of SZ grains reveals dislocation arrays. Figure 11(c) and (d) show higher magnification BF STEM micrographs of AFSP Alloy 282 processed using high- and low-heat input FSP parameters, respectively. Comparing the material processed using high-heat input compared to low-heat input samples, dislocations are clearly visible as sporadic tangles with large defect-free regions separating the tangles. The defect structure of the high-heat input sample appears similar to TEM results presented by Sato et al. [21] for IN600 which contained only a slightly higher dislocation density compared to the mill annealed base material.

Recovery and recrystallization processes are expected to eliminate many of the dislocations introduced as deformation occurs during AFSP. This is especially valid for the high-heat input sample. However, the density of dislocations for the high-heat input sample is overall qualitatively lower compared to the low-heat input sample which exhibits many more dislocations arranged in denser networks. Both samples exhibit a heterogeneous distribution of dislocations with some grains containing a much more extensive dislocation network, suggesting incomplete recovery/recrystallization or the occurrence of some post-recrystallization deformation. STEM BF micrographs showing the distribution of dislocations is in agreement with misorientation analyses discussed previously, the results of which also suggest a locally heterogeneous distribution of stored energy. The difference in stored energy that arises from process parameter-dependent thermomechanical histories accounts for the observed variation in precipitate formation kinetics manifested as a significant difference in heat treatment response and measured microhardness.

Conclusions

A new AFSP was explored for Haynes Alloy 282 using an INCONEL^{TM} Alloy 600 substrate. This new process was successful in creating a consolidated γ'-strengthened superalloy surface layer on a non-age-hardenable substrate after an abbreviated aging heat treatment. The following conclusions were obtained from this study.

1. Hardness in the additive surface layers was increased as much as 100 $HV_{0.3}$ relative to Alloy 600 base material. Low-heat input AFSP parameters resulted in the most dispersed distribution of Alloy 282 within the SZ as well as the highest hardness of the additive Alloy 282.
2. Hard regions in the as-AFSP SZ ($HV_{0.3} > 275$) corresponded to locations within the microstructure containing lamellar distributions of γ'. Thermal simulation of the Alloy 282 weld overlay indicates that γ' forms in the microstructure near the SZ edge where segregation in the weld overlay was only partially homogenized.
3. AFSP of Alloy 282 improved the heat treatment response of resultant surface layers. Additive FSP SZ hardness was measured to be in excess of 400 $HV_{0.3}$ compared to an average of 305 $HV_{0.3}$ for as-deposited Alloy 282 subjected to an aging heat treatment.
4. Electron backscatter diffraction misorientation analyses indicate a higher degree of stored energy in AFSP material processed using low-heat input conditions. Direct observation of dislocations via TEM corresponds to EBSD misorientation analyses. The higher stored energy of the low-heat input condition likely accounts for the observed increase in microhardness and aging response relative to the high-heat input AFSP conditions.

Acknowledgments This study was supported by the Air Force Research Laboratory under the auspices of the Intelligent Manufacturing Initiative. The authors would like to thank the AFRL program manager, Dr. Rollie Dutton. The authors would also like to thank Jennifer Carter and Hallee Deutchman for their FIB and TEM expertise.

References

1. Z.Y. Ma, Friction stir processing technology: a review. Met. Mater. Trans. A **39**, 642–658 (2008)
2. R.S. Mishra, Z.Y. Ma, Friction stir welding and processing. Mater. Sci. Eng. R **50**, 1–78 (2005)
3. J. Newkirk, R.S. Mishra, J. Thomas, J. Hawk, Friction stir powder processing to create surface composites. Adv. Powder Metall. Part. Mater. 797–807 (2003)
4. L.B. Johannes, L.L. Yowell, E. Sosa, S. Arepalli, R.S. Mishra, Survivability of single-walled carbon nanotubes during friction stir processing. Nanotechnology **17**, 3081–3084 (2006)
5. R.S. Mishra, Z.Y. Ma, I. Charit, Friction stir processing: a novel technique for fabrication of surface composite. Mater. Sci. Eng. A **341**, 307–310 (2003)
6. S.M. Mousavizade, F.M. Ghaini, M.J. Torkamany, J. Sabbaghzadeh, A. Abdollah-zadeh, Effect of severe plastic deformation

on grain boundary liquation of a nickel-base superalloy. Scripta Mater. **60**, 244–247 (2009)
7. O.M. Barabash, R.I. Barabash, G.E. Ice, Z. Feng, D. Gandy, X-ray microdiffraction and EBSD study of FSP induced structural/phase transitions in a Ni-based superalloy. Mater. Sci. Eng. A **524**, 10–19 (2009)
8. R.S. Mishra, M. Mahoney, *Friction Stir Welding and Processing* (ASM International, Materials Park, 2007)
9. S. Behrouzghaemi, R.J. Mitchell, Morphological changes of [gamma]' precipitates in superalloy IN738LC at various cooling rates. Mater. Sci. Eng. A **498**, 266–271 (2008)
10. R.C. Reed, *The Superalloys: Fundamentals and Applications* (Cambridge University Press, Cambridge, 2006)
11. X. Sauvage, A. Dede, A.C. Munoz, B. Huneau, Precipitate stability and recrystallisation in the weld nuggets of friction stir welded Al–Mg–Si and Al–Mg–Sc alloys. Mater. Sci. Eng. A **491**, 364–371 (2008)
12. L.M. Pike, *ASME. HAYNES (R) 282 (TM) Alloy—A New Wrought Superalloy Designed for Improved Creep Strength and Fabricability* (American Society of Mechanical Engineers, New York, 2006)
13. D.C. Tung, J.C. Lippold, Weld solidification behavior of Ni-base superalloys for use in advanced supercritical coal-fired power plants, in *Superalloys 2012: 12th International Symposium on Superalloys*, ed. by E.S. Huron, R.C. Reed, M.C. Hardy, M.J. Mills, R.E. Monetero, P.D. Portella, et al. (Seven Springs Mountain Resort, Seven Springs, 2012)
14. J.M. Rodelas, *Friction Stir Processing of Ni-Base Alloys* (Ohio State University, Columbus, OH, 2012)
15. M. Farvizi, S. Asgari, Effects of cold work prior to aging on microstructure of AEREX^{TM}350 superalloy. Mater. Sci. Eng. A **480**, 434–438 (2008)
16. W.C. Liu, Z.L. Chen, F.R. Xiao, S.G. Wang, M. Yao, Strain induced precipitation of gamma ''phase and the gamma" → delta transformation in Inconel 718. Z. Metallk. **90**, 147–152 (1999)
17. J. DuPont, J.C. Lippold, S.D. Kiser, *Precipitation-Strengthened Ni-base Alloys. Welding Metallurgy and Weldability of Nickel-Base Alloys* (Hoboken, Wiley, 2009), pp. 157–254
18. M. Kamaya, A.J. Wilkinson, J.M. Titchmarsh, Measurement of plastic strain of polycrystalline material by electron backscatter diffraction. Nucl. Eng. Des. **235**, 713–725 (2005)
19. A.J. Wilkinson, Measuring strains using electron backscatter diffraction, in *Electron Backscatter Diffraction in Materials Science*, ed. by A.J. Schwartz, M. Kumar, B.L. Adams (Kluwer Academic/Plenum Publishers, New York, 2000), pp. 231–246
20. E.M. Lehockey, Y. Lin, O.E. Lepik, Mapping residual plastic strain in materials using electron backscatter diffraction, in *Electron Backscatter Diffraction in Materials Science*, ed. by A.J. Schwartz, M. Kumar, B.L. Adams (Kluwer Academic/Plenum Publishers, New York, 2000)
21. Y.S. Sato, P. Arkom, H. Kokawa, T.W. Nelson, R.J. Steel, Effect of microstructure on properties of friction stir welded Inconel Alloy 600. Mater. Sci. Eng. A-Struct. Mater. Prop. Microstruct. Process. **477**, 250–258 (2008)